Published in IET Microwaves, Antennas & Propagation
Received on 6th May 2009
Revised on 25th September 2009
doi: 10.1049/iet-map.2009.0281

ISSN 1751-8725

Intermodulation distortion in narrowband amplifier circuits

G.J. Mazzaro M.B. Steer K.G. Gard

Department of Electrical and Computer Engineering, North Carolina State University, Raleigh, NC 27695-7914, USA
E-mail: gjmazzar@ncsu.edu

Abstract: The contribution of bandpass filter memory to intermodulation distortion in narrowband amplifier circuits is examined. A method for generating multisines from filtered switched tones is presented, and techniques for measuring an amplifier's IP3 and extracting a filter's passband using these multisines are developed. It is shown that amplified filtered pulses produce intermodulation distortion in frequency-hopping communication systems. In the experimental study, 465 and 900-MHz Chebyshev bandpass filters are considered.

1 Introduction

Intermodulation distortion (IMD) is a fundamental performance metric for radio-frequency (RF) and microwave devices. Such distortion results when any circuit containing a non-linearity is subjected to multiple simultaneous input frequencies, or 'multisines', whose interactions at the non-linearity produce harmonics that are integer combinations of the original frequencies. IMD is particularly vexing to RF front-ends because (a) some of the intermodulation products fall within the intended communications band, (b) new sources of IMD continue to be discovered and (c) even when IMD does appear and its source can be identified, it is difficult to mitigate.

IMD in bandpass circuits has several causes. Passive filters themselves exhibit weak non-linearities which result from conductor defects and uneven charge carrier densities [1, 2]. Distortion in active filters which use negative-resistance compensation is produced by transistor non-linearities [3, 4]. We have observed another source of IMD in amplifier circuits that use bandpass filtering, which disappears if the filter is absent. This IMD can be traced to waveform memory retained as stored reactive energy within the filter.

The IMD resulting from this memory effect may be exploited for circuit metrology. One example is the measurement of amplifier non-linearity. Because linear filtering effects are known to produce multitone interference when excited by switched tones [5], it is possible to perform non-linear tests requiring multiple simultaneous frequencies with a single switched-tone source. This paper presents a switched-tone technique for measuring an amplifier's third-order intercept point (IP3).

The memory effect may also be used to characterise the filter itself. Most techniques for characterising resonant circuits assume that the structure simplifies to a single, linear resonator in the frequency band of interest [6]. These techniques are insufficient, however, when the circuit contains multiple coupled resonators with overlapping frequency bands. The characterisation reported in this paper, which determines a filter's passband from a single input port, is a non-linear method, which may be extended to any number of coupled resonators.

Distortion related to filtering also has implications for communication system performance. The IMD produced by filters alone is known to cause interference in systems with multiple simultaneous users operating on different frequencies, as in orthogonal frequency division multiplexing (OFDM) [1]. The IMD produced by a filter–amplifier cascade may also cause interference in systems with multiple users time-multiplexed to different frequencies, as in frequency-hopping spread spectrum (FHSS) systems such as *ad-hoc* networks and WiFi™. This paper extends the work done by the authors on co-site interference produced by linear filtering to non-linear distortion produced by pairing a bandpass filter with an amplifier, as in a typical RF front-end. Results show that

© The Institution of Engineering and Technology 2010

the transmissions which produce IMD need not originate within the intended communications band.

2 Multisines from switched tones

The resonant properties of bandpass filters produce transient effects that are not widely known. One such effect is the output of multi-tone interference from the application of switched-tone pulses [5]. Another effect is the output of steady-state multisines from the application of repetitive switched tones. In this section, the mathematics which model the switched-tone to multisine conversion are presented, along with measurements which confirm the effect and a discussion of filter energy storage which explains the observed phenomenon.

2.1 Switched-tone to multi-tone theory

Let the input to a bandpass filter (BPF) be the switched-tone signal given by

$$v_i(t) = \sum_{n=1}^{N} A_n \cos(\omega_n t + \phi_n) s(t - T[n-1]/N) \quad (1)$$

where ω_n are the frequencies of the tones, A_n are their amplitudes, ϕ_n are their initial phases and $s(t)$ is the periodic switching waveform given by

$$s(t) = u(t) - u(t - T/N) = s(t + T) \quad (2)$$

where T is the switching period. The circuit for $N = 2$, which converts a two-tone switched signal into a two-tone multisine, is given in Fig. 1.

The Fourier transform of $s(t)$ is

$$S(\omega) = \sum_{k=-\infty}^{+\infty} \frac{2\sin(k\pi/N)}{k} \delta(\omega - k\omega_s) \quad (3)$$

where $\omega_s = 2\pi/T$ is the switching frequency; thus, the Fourier transform of the input voltage $v_i(t)$ is

$$V_i(\omega) = \sum_{k=-\infty}^{+\infty} \frac{\sin(k\pi/N)}{k} \sum_{n=1}^{N} \left\{ \begin{array}{l} A_n \, e^{j\phi_n} \, e^{-j\omega T[n-1]/N} \\ \times [\, \delta(\omega - k\omega_s - \omega_n) \\ \quad + \delta(\omega - k\omega_s + \omega_n)] \end{array} \right\} \quad (4)$$

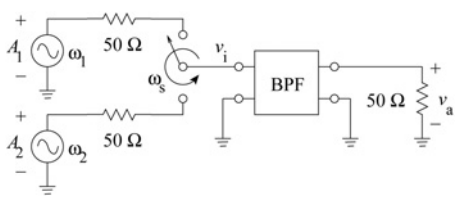

Figure 1 *Circuit for converting two switched tones into a two-tone multisine*

Let $S_{21}(\omega)$ be the filter's forward transmission characteristic. If the switching frequency is much greater than the filter bandwidth, $\omega_s \gg B$, such that only the $k = 0$ terms from (4) are passed, then the filtered sum reduces to

$$V_a(\omega) = \sum_{n=1}^{N} \frac{A_n}{N} e^{j\phi_n} S_{21}(\omega_n) \left[\begin{array}{l} \pi\delta(\omega - \omega_n) \\ + \pi\delta(\omega + \omega_n) \end{array} \right] \quad (5)$$

whose time-domain equivalent is

$$v_a(t) = \sum_{n=1}^{N} \frac{A_n}{N} |S_{21}(\omega_n)| \cos \left[\begin{array}{c} \omega_n \left(t - \frac{T}{N}[n-1] \right) \\ + \phi_n + \theta(\omega_n) \end{array} \right] \quad (6)$$

where $\theta(\omega) = \arg\{S_{21}(\omega)\}$. The filtered output of the switched-tone input is a multisine signal. Each tone's amplitude is proportional to its original amplitude A_n, reduced by the switching duty cycle $1/N$, and multiplied by the filter's amplitude characteristic at ω_n. Each tone's phase is equal to its original phase ϕ_n, plus the switching delay $T[n-1]/N$, plus the filter's phase characteristic at ω_n.

2.2 Measurements

A measurement system which demonstrates the switched-tone to multisine conversion is shown in Fig. 2. The Agilent E8267C functions as the tone generator and switch; it outputs two tones, spaced 100 kHz apart, centred at $f_0 = 465$ MHz, with a switching frequency of $f_s = 40$ MHz. The filter is a low-ripple Chebyshev design, seventh order, with a centre frequency of 465 MHz and an insertion loss (IL) of 9.75 dB. The Tektronix TDS684B oscilloscope records the time-domain waveforms. Measured data are shown in Fig. 3.

The switched-tone input to the filter is shown in Fig. 3*a*. It has a nearly constant envelope, with some amplitude modulation. The residual modulation is due to the 80 MHz modulation bandwidth of the E8267C synthesiser, that is, this waveform is a digitised version of the ideal switching waveform v_a with a bandwidth of only 80 MHz. A wider modulation bandwidth would contain a greater number of switching harmonics from (4) and produce a more constant envelope.

The multisine output from the filter is shown in Fig. 3*b*. This plot displays a classic two-tone multisine pattern, whose amplitude has been attenuated from the input waveform by the 50% duty cycle of the switching

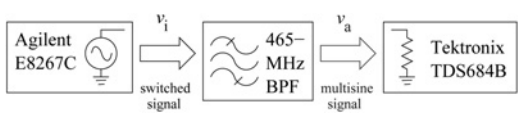

Figure 2 *Test setup for switched-tone to multisine conversion*

© The Institution of Engineering and Technology 2010
IET Microw. Antennas Propag., 2010, Vol. 4, Iss. 9, pp. 1149–1156
doi: 10.1049/iet-map.2009.0281

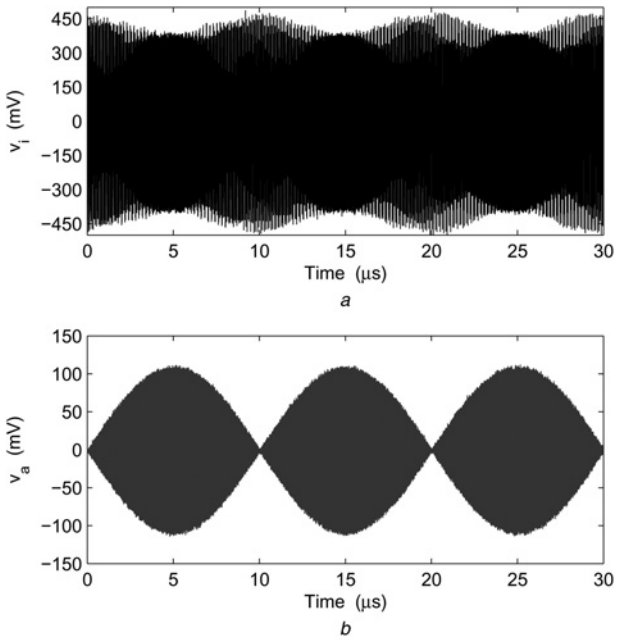

Figure 3 *Measured time-domain illustration of switched-tone to multisine conversion using 7th-order 465-MHz 1% filter*

a Input to filter
b Output of filter
The filter's insertion loss is 9.75 dB

mechanism and by the insertion loss of the filter. The switched-tone to multi-tone conversion is confirmed.

2.3 Discussion

The mathematics of Section 2.1 does not imply the physical mechanism of the switched- to multi-tone conversion. The multisine output can be explained, however, by studying filter energy storage. Several simulations in Advanced Design System (ADS) 2006 provide insight into bandpass filter behaviour. Fig. 4 is a sample of these simulations.

The circuit of Fig. 1 is simulated using a seventh-order 465-MHz 3%-bandwidth filter. The first simulation is performed with only one tone active ($A_2 = 0$). The filter input is shown in Fig. 4*a*, whereas the filter output corresponding to this input is shown in Fig. 4*b*.

The pulsed filter response is somewhat counter-intuitive. Whereas the input displays clear intervals where the signal is absent, the filtered output shows no time during which the signal is absent. Although the input to the filter is sometimes switched completely off, the filter output never decays.

The lack of decay in the output can be attributed to the speed at which the input signal changes relative to the speed at which the bandpass filter responds. The response time of the filter is on the order of $1/B$, whereas the

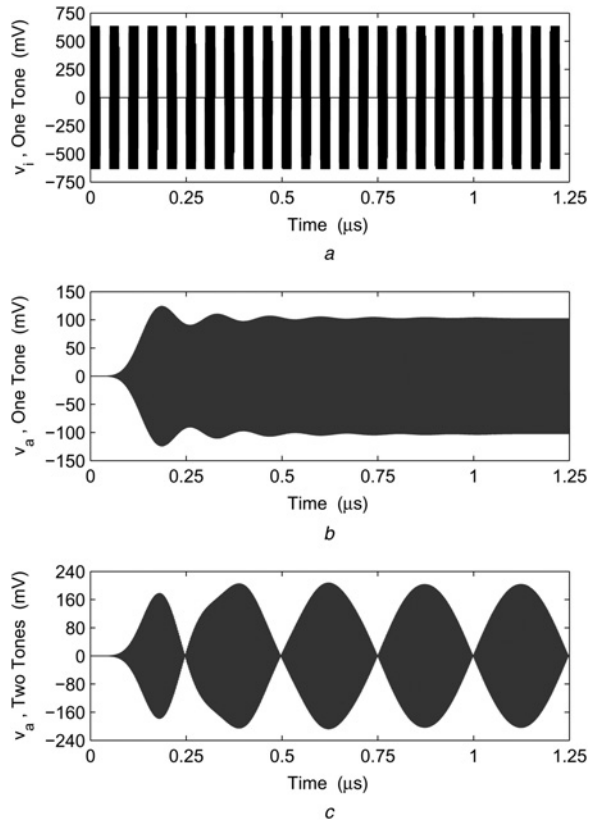

Figure 4 *Simulated pulse response of seventh-order 465-MHz 3% Chebyshev filter*

a Input to filter with only f_1 active
b Output from filter with only f_1 active
c Output from filter with f_1 and f_2 active
$P_i = 0$ dBm/tone in each case, $f_s = 20$ MHz, filter IL = 9.75 dB

switching period is $1/f_s$. Since the switching frequency is much higher than the filter bandwidth, the response time of the filter is much slower than the switching speed. The input switches on and off faster than the time required to charge the resonant sections of the filter.

Applying a series of pulses in this manner forces the filter sections to build resonance, albeit at a slower rate than using longer pulses, without giving the resonant sections time to discharge between each pulse. For this reason, applying a single on–off tone at the filter input produces a steady single tone at its output (after its initial transient) as shown in Fig. 4*b*. A second on–off tone applied to the input, shifted in time by half of the switching period, produces a similar steady single tone at the output, with a phase shift of half the switching period by (6). Adding both inputs produces a constant-envelope switched-tone stimulus, while adding both outputs produces a two-tone multisine, as shown in Fig. 4*c*. The filter charges to a steady state at any passband frequency, regardless of the time-offset of its input, as long as the input switches faster than its transient response; thus, by rotating through switched tones at its input, any number of multi-tones may be produced at its output.

© The Institution of Engineering and Technology 2010

3 IP3 measurement with switched tones

One useful feature of the switched-tone to multisine conversion is the ability to perform multi-tone measurements using single-frequency synthesisers. In those instances when a multisine source is not available, multiple single-tone sources, a switch and a narrowband filter will suffice.

An example of such a measurement is that of output IP3. Such a measurement is typically performed on an amplifier or mixer by applying a two-tone source at the input with a small tone separation (1 MHz or less), sweeping the input power at a fixed frequency and plotting the linear output power and intermodulation power on the same logarithmic axes [7]. The IP3 is found by extrapolating the linear data from the region where the amplifier provides a constant gain over power for the fundamental tones, extrapolating the non-linear data from the region where the amplifier provides 3 dB of additional non-linear power for every 1 dB of linear power, and finding the intersection of the two extrapolations. An example of this technique is shown in Fig. 5. The intersection takes place at $P_o = 53$ dBm, so this is the measured IP3 of the amplifier.

The measurement given in Fig. 5 is unique, however, because the data was generated using a switched-tone setup as given in Fig. 6. The Agilent E8267C provided the switched tones, and the filter frequencies were chosen to be within the amplifier's operational bandwidth. A 20-dB coupler was used to tap off a portion of the amplifier's output signal so as not to damage the spectrum analyser by feeding it excessive power.

Table 1 lists the IP3 values provided by the manufacturer's datasheets, measured IP3 using the traditional steady-state technique, and measured IP3 using the switched-tone technique for three different amplifiers. (The MiniCircuits ZRL3500 amplifier was measured with a fifth-order 2-GHz 1% filter with tones at $f_1 = 1999.5$ MHz and $f_2 = 2000.5$ MHz. The RFMD RF2320 amplifier was measured with a fifth-order 1-GHz 2% filter with tones at $f_1 = 999.5$ MHz and $f_2 = 1000.5$ MHz.) The steady-state technique gives values within 9% of the datasheet values, whereas the switched-tone technique gives values within 10%. The switched-tone technique is nearly as accurate as the steady-state technique.

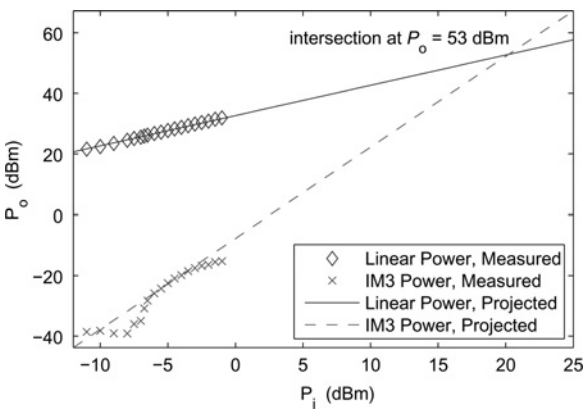

Figure 5 *Output third-order intercept measurement for Ophir 5162 amplifier: switched tones with seventh-order 900-MHz 3% filter, f_1 =899.5 MHz, f_2 =900.5 MHz, f_s = 40 MHz*

The amplifier datasheet reports its 'typical IP3' as 54 dBm

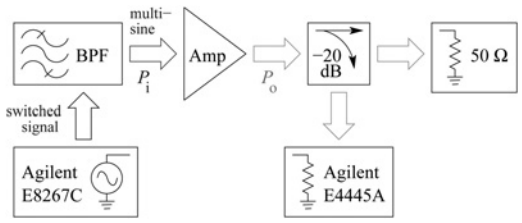

Figure 6 *Test setup for output IP3 measurement*

All measurements are taken with $f_2 - f_1 = 1$ MHz and $f_s = 40$ MHz

Table 1 IP3 measurement: two-tone against switched-tone

Amplifier	IP3 from datasheet, dBm	IP3 from two-tone, dBm	IP3 from switched-tone, dBm
MiniCircuits ZRL3500	42	43.1	42.8
Ophir 5162	54	53.8	52.9
RFMD RF2320	34	36.8	37.2

4 One-port filter passband extraction

Another consequence of the multisine conversion is the ability to perform a two-port measurement on a bandpass filter using a single input port. Because multiple simultaneous tones may be generated at the filter output, it is not only possible to transmit intermodulation to the output of a non-linearity in cascade with the filter, it is also possible to reflect intermodulation from the input of such a non-linearity, transmit it back through the filter and measure it when it returns to the filter's input port. The non-linear reflection is present only in the retransmission, whereas linear reflections are generated by both the filter and the amplifier. The linear reflections are not separable at the filter input port. For this reason, only the non-linear frequency content is able to provide two-port data from the single-port measurement [8]. This section will present the mathematics that govern the non-linear reflection and will provide measured data that show that it is possible to extract the operational bandwidth of a filter using an appropriate frequency sweep.

© The Institution of Engineering and Technology 2010
IET Microw. Antennas Propag., 2010, Vol. 4, Iss. 9, pp. 1149–1156
doi: 10.1049/iet-map.2009.0281

4.1 Passband extraction theory

The circuit used to extract bandpass filter transmission frequencies is shown in Fig. 7. The signal path from v_i to v_r resembles the filter-non-linearity-filter path from prior studies of bandpass non-linearities [9, 10]. Here, the filters on either side of the non-linearity (NL) are the same circuit, with the input and output reversed.

The signal power transmitted through the filter to the non-linearity is

$$P_a(\omega) = |S_{21}(\omega)|^2 P_i(\omega) \tag{7}$$

Let the amount of linear power transmitted to the non-linearity which is converted to reflected intermodulation power in the fundamental zone be

$$\tilde{P}_b(\omega) = 10^{\alpha} P_a(\omega)^{\beta} \tag{8}$$

where α is a logarithmic scaling factor, β is the order of the non-linearity and the tilde above P_b denotes intermodulation. For a two-tone signal, $P_a(\omega)$ is non-zero only at ω_1 and ω_2, while $\tilde{P}_b(\omega)$ is non-zero only at $\omega_{\text{avg}} \pm \Delta\omega(2m+1)/2$ where

$$\omega_{\text{avg}} = \frac{\omega_1 + \omega_2}{2}, \quad \Delta\omega = \omega_2 - \omega_1, \quad m = 0, 1, 2, \ldots \tag{9}$$

If $S_{12}(\omega)$ is the filter's reverse transmission characteristic, then the non-linear power retransmitted through the filter is given by

$$\tilde{P}_r(\omega) = |S_{12}(\omega)|^2 \tilde{P}_b(\omega) \tag{10}$$

It is assumed that the filter itself is linear. For filters that are also reciprocal, $S_{12} = S_{21}$. For many front-end bandpass filters, the approximation $|S_{12}| \simeq |S_{21}|$ is sufficient. Using this approximation and substituting (7) into (8) and (8) into (10) gives

$$\tilde{P}_r(\omega) = 10^{\alpha} |S_{21}(\omega)|^{2(\beta+1)} P_i(\omega)^{\beta} \tag{11}$$

which states that the intermodulation power reflected from the filter-non-linearity cascade is the product of the input linear power raised to the order of the non-linearity β, the filter's power transmission raised to $\beta + 1$, and a logarithmic scaling factor α.

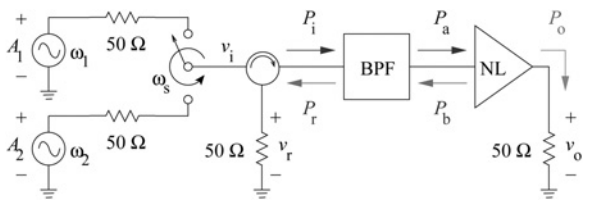

Figure 7 *Circuit for extracting filter passband from non-linear reflections*

The values of α and β may be determined by rewriting (11) as

$$\log \tilde{P}_r(\omega) = \beta \log P_i(\omega) + (\beta + 1) \log |S_{21}(\omega)|^2 + \alpha \tag{12}$$

By plotting $\log \tilde{P}_r(\omega)$ at different input power levels $\log P_i(\omega)$, the rightmost two terms in (12) remain constant, and β is the slope of this plot. If the filter is assumed to be lossless, then α will be the y-intercept of this same plot when the input tones are within the filter passband, that is, when $S_{21} = 1$ such that the middle term of (12) vanishes. If the filter cannot be assumed lossless, then α is not easily determined; however, since the goal of this procedure is to extract the filter passband and not its insertion loss, the value of α is not critical.

The filter passband is extracted by plotting $\log \tilde{P}_r(\omega)$ over frequency at a constant input power. For constant input power, the first and third terms of (12) contribute a DC offset to the trace, whereas the second term traces out the power transmission characteristic of the filter (scaled by $\beta + 1$).

4.2 Measurements

A measurement system that demonstrates the passband extraction is shown in Fig. 8. The same Agilent E8267C unit is the switched-tone source, and the Ophir 5162 broadband amplifier is used to boost the linear power to a suitable level to excite the non-linearity. A circulator transmits the switched-tone probe to the filter input port and redirects reflections from the filter–amplifier cascade to the Agilent E4445A spectrum analyser. The filter output port is connected to the Philips BGA2648 amplifier, which is terminated in 50 Ω (not shown). The Philips amplifier was chosen as the non-linearity so that its relatively low input IP3 would accentuate the intermodulation response. Three 900-MHz filters with different bandwidths were tested.

Fig. 9 shows a plot of average reflected IM3 ($m = 2$) power against frequency for the three filters. Each subfigure of Fig. 9 contains a scaled, attenuated version of the filter's transmission characteristic S_{21} for comparison to the theory of Section 4.1. With the exception of the dips at the centre of the passbands for the 3% and 5% filters, the shapes of the reflected intermodulation power traces and the scaled

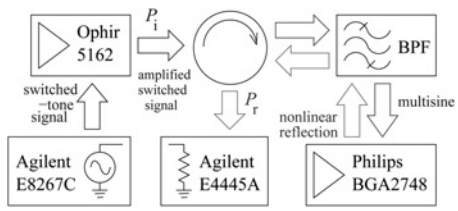

Figure 8 *Test setup for filter passband extraction*

The non-linearity is the BGA2748 amplifier which has an input IP3 of −24 dBm at 900 MHz and is powered by a 4-Volt supply

© The Institution of Engineering and Technology 2010

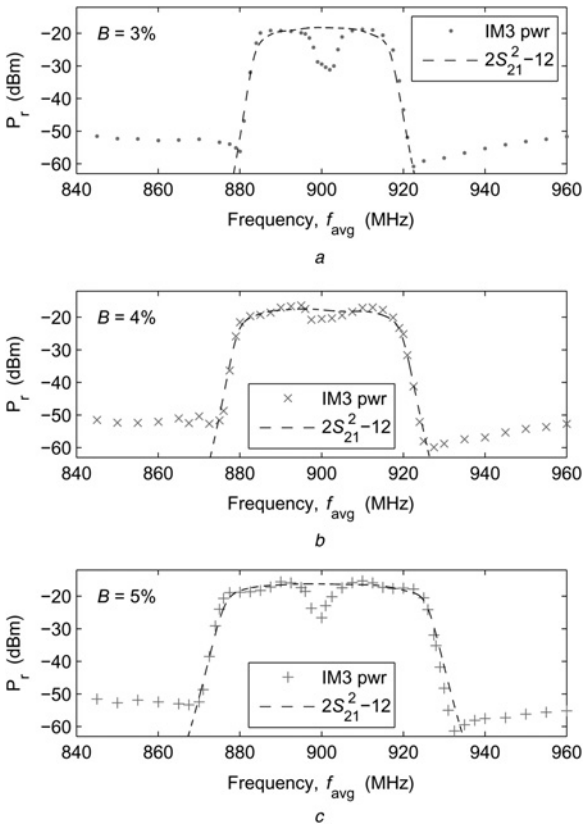

Figure 9 *Passband extraction for three seventh-order 900-MHz Chebyshev filters*

a 3% Bandwidth
b 4% Bandwidth
c 5% Bandwidth
$P_i = 18$ dBm/tone, $f_{avg} = \omega_{avg}/2\pi$, $f_2 - f_1 = 100$ kHz, $\alpha = -12$, $\beta = 1$. P_r is the average IM3 power. The non-linearity is the Philips BGA2748 amplifier. Scaled, attenuated S_{21} for each filter included for comparison

filter transmission characteristics match very well in the expected communications band. The passband of each filter is readily identified from these frequency sweeps. Similar identification may be performed on filters in other communications bands so long as the frequency sweeps can be made to encompass the passbands.

5 IMD in frequency-hopping systems

Although filter memory enables multisine testing and filter characterisation, there are notable negative consequences to the multisine conversion. One such consequence is the signal-to-noise degradation in a frequency-hopping scheme which implements a high-order filter in its receiver [5]. Another consequence is the IMD produced in a similar scheme which amplifies the signal after filtering it. This section will explain the origin of this distortion and will present measurements which confirm its existence in a frequency-hopping scenario.

5.1 Origin of IMD in frequency-hopping

A switched-tone signal consisting of a single switch between two frequencies, when applied to a bandpass filter, is known to produce two-tone interference at the filter output for particular input frequency combinations. This is because wave energy at different frequencies travels through the filter at different speeds, so that an interference pattern may be produced at the filter output by inputting a frequency that travels slowly through the filter and switching to a frequency that travels quickly through the filter [5].

Despite the transitory nature of the single switching event, a multisine waveform will still exist at the filter output and this multisine signal will be applied to an amplifier that follows the filter, which in turn produces IMD at its output because of its inherent non-linearity. Similar to the way the steady-state two-tone excitation produced the steady-state intermodulation discussed in Sections 3 and 4, here a transient two-tone pattern produces transient intermodulation. Such intermodulation is detrimental to a communications system because the IMD frequencies are often inside or nearby the intended communications band.

5.2 Measurements

A measurement system that demonstrates IMD generated in a frequency-hopping scenario is shown in Fig. 10. The Agilent E4438C synthesiser acts as User 1 transmitting data at carrier frequency f_1 whereas the Agilent E8267C synthesiser acts as User 2 transmitting data at carrier frequency f_2 (or, equivalently, User 1 transmitting data after having hopped to frequency f_2 from f_1). The MiniCircuits ZFSWA-2-46 switch time-multiplexes the two users to the 900-MHz filter and Ophir 5162 amplifier which act as the RF front-end of the receiver. The average IM3 power (divided by the average fundamental tone power) recorded by the Agilent E4445A for several combinations of user frequencies is plotted with a greyscale colormap in Fig. 11.

A number of results in Fig. 11 are worth noting. First, the intermodulation generated by users whose frequencies are within or near the filter band is always above −120 dBc and is sometimes as high as −83 dBc. The highest levels of distortion are recorded for starting frequencies near the filter passband edges and ending frequencies well inside the

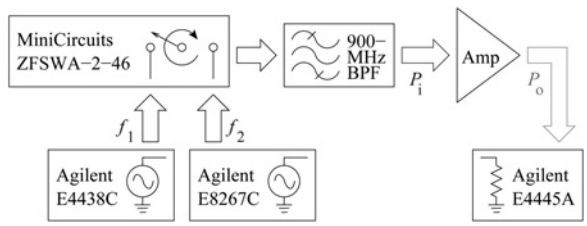

Figure 10 *Test setup for frequency-hopping IMD: the filter is seventh-order at 900-MHz with 3% bandwidth; the amplifier is the Ophir 5162 at 90% gain*

© The Institution of Engineering and Technology 2010
IET Microw. Antennas Propag., 2010, Vol. 4, Iss. 9, pp. 1149–1156
doi: 10.1049/iet-map.2009.0281

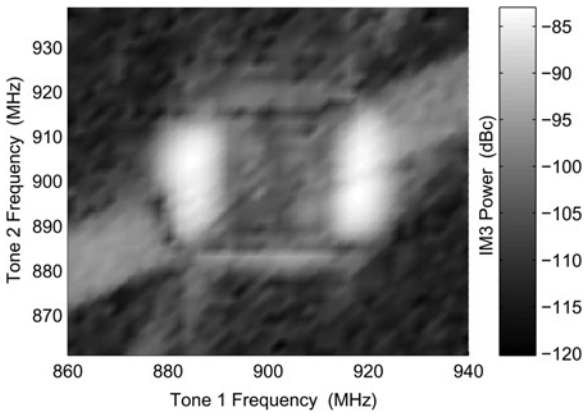

Figure 11 *IMD for single switching event: tone 1 is applied for 112 ns, then tone 2 is applied for 112 ns, then both are switched off for 226 ns; $P_i = -11$ dBm/tone*

The passband of the filter is 885–915 MHz

passband (e.g. $f_1 = 887$ MHz, $f_2 = 900$ MHz). This trend is expected, though, because of the aforementioned dependence of signal speed on input frequency: by switching to a 'faster' frequency after a 'slower' one, a greater degree of multi-tone interference is produced at the filter output, resulting in a greater amount of distortion generated by the amplifier. Second, the IMD is no less than −110 dBc for frequency combinations well within the filter's rated passband. This result means that users transmitting inside the communications band generate distortion in the receiver front-end at frequencies within the communications band. This distortion is then termed co-site interference. Third, there is considerable distortion recorded for frequencies outside the filter passband. The grey stripes in the lower-left and upper-right corners of Fig. 11 contain frequency combinations well outside the filter passband whose IMD is generally above −100 dBc. This result means that users transmitting outside the communications band still generate distortion in the receiver front-end at frequencies outside the communications band, despite the expected attenuation of these frequencies by filtering. Fourth, there exist many combinations of frequencies, one outside the filter passband and one inside the filter passband, which will generate IMD in the receiver front-end at frequencies within the communications band (e.g. $f_1 = 882$ MHz, $f_2 = 890$ MHz, $2f_2 - f_1 = 898$ MHz). This result means that it is possible for a transmitter operating in one channel to cause IMD within the communications band of a receiver operating in an adjacent channel if the pulse transitions within the two channels take place at approximately the same time.

In summary, the data show that a communications scheme which implements a filter–amplifier cascade and whose received data come from different frequencies in adjacent time slots, whether they are within the communications band or not, is subject to IMD caused by filter memory. The intermodulation frequencies are calculable from the user frequencies, and the degree of distortion is related to the frequencies as well as the order in which they are used.

The data presented in Fig. 11 are a worst-case scenario for a frequency-hopping scheme which places no guard-band between user pulses. One way to reduce the amount of distortion is to place a waiting period between user transmissions, which will lessen the pulse overlap caused by the filter transient and cut down on the multi-tone interference presented to the amplifier input, thereby reducing the distortion generated at the amplifier output.

6 Conclusions

Although circuit measurements have traditionally been performed using linear and steady-state methods, additional information may be obtained by using non-linear and transient methods. Resonant energy storage, while generally not an intended behaviour, is always present when signals are applied to bandpass filters. This energy storage, along with both time- and frequency-domain analysis, enables circuits to be measured in ways that are not possible in linear steady state.

Unfortunately, this energy storage property has drawbacks, particularly for communications systems which employ frequency-switching in addition to filtering. Switching between frequencies may lead to distortion at the transitions between pulses because of the overlap caused by filter memory. Care must be taken so that a bandpass filter, which is designed to block extraneous frequency content, does not itself create interference within its intended communications band.

7 Acknowledgments

This material is based upon work supported by the U.S. Army Research Office under grant number W911NF-07-1-0004 and as a Multi-disciplinary University Research Initiative under grant number W911NF-05-1-0337.

8 References

[1] SALKOLA M.I.: 'Intermodulation response of superconducting filters', *J. Appl. Phys.*, 2005, **98**, (2), pp. 023907–023907-13

[2] VENDIK O.G., VENDIK I.B., SAMOILOVA T.B.: 'Nonlinearity of superconducting transmission line and microstrip resonator', *IEEE Trans. Microw. Theory Tech.*, 1997, **45**, (2), pp. 173–178

[3] CHENG K.M., CHAN S.C.: 'Reduction of intermodulation distortion in microwave active bandpass filters–theory

© The Institution of Engineering and Technology 2010

and experiments', *IEEE Trans. Microw. Theory Tech.*, 2000, **48**, (2), pp. 221–225

[4] HUNTER I.C., CHANDLER S.R.: 'Intermodulation distortion in active microwave filters', *IEE Proc. Microw. Antennas Propag.*, 1998, **145**, (1), pp. 7–12

[5] MAZZARO G.J., STEER M.B., GARD K.G., WALKER A.L.: 'Response of RF networks to transient waveforms: Interference in frequency-hopped communications', *IEEE Trans. Microw. Theory Tech.*, 2008, **56**, (12), pp. 2808–2814

[6] MAZZARO G.J., STEER M.B., GARD K.G.: 'Filter characterisation using one-port pulsed RF measurements', *IET Microw. Antennas Propag.*, 2009, **3**, (2), pp. 303–309

[7] PEDRO J.C., CARVALHO N.B.: 'Intermodulation distortion in microwave and wireless circuits' (Artech House, Boston, MA, 2003)

[8] WALKER A.L.: 'Behavioral modeling and characterisation of non-linear operation in RF and microwave systems'. PhD thesis, North Carolina State University, 2005

[9] BLACHMAN N.M.: 'Band-pass non-linearities', *IEEE Trans. Inf. Theory*, 1964, **10**, (2), pp. 162–164

[10] LYONS R.G.: 'Signal and interference output of a bandpass non-linearity', *IEEE Trans. Commun.*, 1979, **27**, (6), pp. 888–891

© The Institution of Engineering and Technology 2010
doi: 10.1049/iet-map.2009.0281